Nonlocal Pair Correlations in a Higher-Order Bose Gas Soliton

King Lun Ng and Bogdan Opanchuk
Centre for Quantum and Optical Science, Swinburne University of Technology, Melbourne 3122, Australia

Margaret D. Reid and Peter D. Drummond
Centre for Quantum and Optical Science, Swinburne University of Technology, Melbourne 3122, Australia
and Institute of Theoretical Atomic, Molecular and Optical Physics (ITAMP),
Harvard University, Cambridge, Massachusetts 02138, USA

(Received 15 November 2018; published 20 May 2019)

The truncated Wigner and positive-P phase-space representations are used to study the dynamics of a one-dimensional Bose gas. This allows calculations of the breathing quantum dynamics of higher-order solitons with $10^3 - 10^5$ particles, as in realistic Bose-Einstein condensation experiments. Although classically stable, these decay quantum mechanically. Our calculations show that there are large nonlocal correlations and nonclassical quantum entanglement.

DOI: 10.1103/PhysRevLett.122.203604

A classical soliton [1,2] is a nondispersive pulse caused by the balance of dispersion and nonlinearity in a nonlinear wave. Their initial shape can be maintained during propagation. Higher-order classical solitons have additional spatiotemporal oscillations. Time invariant quantum solitons can exist [3,4], but are completely delocalized in phase and in space. When a coherent soliton is prepared that is classically invariant, quantum effects change the soliton shape. These have been theoretically predicted [5–7] and experimentally verified [8–11].

Higher-order solitons have attracted much recent interest, since their quantum fluctuations can become macroscopically large [12–16]. This leads to a macroscopic quantum initiated decay with fragmentation into multiple condensates, reminiscent of the decay of a false vacuum in scalar quantum field theory [17]. In this Letter, we show that these quantum effects are accompanied by nonlocal dynamical correlations, which occur even before the soliton decays. These fluctuations are largest for a Bose-Einstein condensate soliton formed at mesoscopic particle number. This may be testable in proposed experiments [15] in bosonic ^{7}Li, with $10^3 - 10^4$ Bose condensed atoms. These correlations survive to very large particle number, and we obtain measurable predictions even for small density changes.

One-dimensional (1D) attractive Bose gases form a bright soliton in photonic [18] and Bose-Einstein condensate environments [19–21]. The classical description is known in optics as the nonlinear Schrödinger equation, and in atomic physics as the Gross-Pitaevskii equation [22–24]. This equation uses a mean-field approximation equivalent to assuming that operator products are factorizable. In order to include the full quantum properties, beyond mean-field methods are needed that include correlations, allowing predictions of rich quantum features. These provide tests of many-body quantum dynamics in a controlled, experimentally accessible environment.

An early prediction in photonic systems was the generation of quantum squeezing and entanglement [5,6] in one-dimensional bright solitons, verified experimentally in photonic experiments [8,9,11]. More recently, there has been interest in the quantum dynamical evolution of higher-order solitons, which oscillate periodically in space at the mean-field level. They can be generated from a fundamental soliton with a sech envelope by a rapid increase in the coupling constant. In atomic gases, this is obtainable through a Feshbach resonance to give a stronger coupling regime with fewer particles than in photonics. Other related studies include a mean-field treatment of quenches [25] and static quantum treatments of solitons in potential wells [26].

Here we use quantum phase space methods to analyze a quench experiment in which the full many-body quantum state is sampled probabilistically, allowing a calculation of the dynamical evolution of nonlocal correlation functions. These are good indicators of entanglement and possible Bell violations in Bose-Einstein condensation (BEC) systems [27–31]. The main technique used is a truncated Wigner (TW) method [32] that employs a $1/N$ expansion for N particles, with $N = 10^3$–10^5, and a Poissonian number variance. The general approach has been verified through accurate predictions of quantum squeezing in optical fiber solitons [5,6,33]. All the local conservation laws of the bright BEC soliton system are preserved [34]. We also confirm these results using the exact positive-P and complex-P phase-space representations [35] up to the first oscillation peak, and with pure number state initial conditions.

The density dynamics, but not correlations, have been calculated previously. An approximate variational prediction [13] using the many-body multiconfigurational time-dependent Hartree for bosons method (MCTDHB) predicted a sudden fragmentation into two equal fragments. Later work [14] pointed out that this MCTDHB approximation failed to predict the known center-of-mass variance growth. This is because the calculation used only two modes, while there are seven or more condensate modes present [16]. Other methods using exact eigenstates [15] or the density matrix renormalization group approximation [36] have several orders of magnitude fewer particles.

For Bose gases strongly confined in a one-dimensional waveguide along the r direction with a transverse trapping frequency $\omega_\perp$, the Hamiltonian in the occupation number representation is given by

$$\hat{H}_{1D} = \int dr \left(\frac{-\hbar^2}{2m} \hat{\Psi}^\dagger \frac{\partial^2}{\partial r^2} \hat{\Psi} + \frac{g}{2} \hat{\Psi}^{\dagger 2} \hat{\Psi}^2 \right), \tag{1}$$

where $\hat{\Psi}(r)$ is a one-dimensional quantum field operator.

The total many-body Hamiltonian includes two-body s-wave collisions where $g = 2\hbar a \omega_\perp$ is the interaction strength. This is tunable, since the s-wave scattering length a is a function of the external magnetic field via a Feshbach resonance [37]. Taking a characteristic length scale r_0, particle number N, and timescale t_0 where $r_0^2 = \hbar t_0 / 2m$, the length, time, and field operator are transformed into dimensionless form where $z = r/r_0$, $\tau = t/t_0$, and $\hat{\psi}(z) = \hat{\Psi}\sqrt{r_0/N}$. The interaction strength g is also transformed into a scaled quantity $C = mgr_0 N/\hbar^2$. The corresponding Hamiltonian [3,38] for a system of dimensionless length L is

$$\hat{h} = \int_0^L dz [-\hat{\psi}^\dagger(z) \nabla_z^2 \hat{\psi}(z) + C \hat{\psi}^{\dagger 2}(z) \hat{\psi}^2(z)]. \tag{2}$$

We assume an initial coherent state [39] for the BEC, which has a Poissonian distribution of particle numbers. This is a good approximation to the lowest observed experimental BEC number fluctuations in small condensates of 10^3 particles [40]. In the Wigner representation, the field operator $\hat{\psi}(z)$ is replaced by an appropriately scaled stochastic field $\psi \sim \hat{\psi}$ [6,41,42], which in a symmetrically ordered mapping is initially

$$\psi(z) = \sqrt{n_0(z)} + \frac{1}{\sqrt{2}} \eta(z). \tag{3}$$

Here $\eta(z)$ is a complex number with correlations $\langle \eta(z)\eta(z') \rangle = 0$ and $\langle \eta(z)\eta^*(z') \rangle = \delta(z-z')/\sqrt{N}$, while $n_0(z) = \langle \hat{\psi}^\dagger(z)\hat{\psi}(z) \rangle$. An alternative approach is to use the positive-P representation [5,35], which is exact, equivalent to normal ordering, and has two stochastic fields ψ, ψ^+ with initial values $\psi(z) = \psi^+(z) = \sqrt{n_0(z)}$.

The Bose gas is assumed to initially have a soliton size that corresponds to a weakly attractive interaction $C = -2$, with $n_0(z) = \mathrm{sech}^2(z)/2$. At time $\tau = 0$, a rapid change of interaction strength is activated by changing the coupling to $C = -8$. These parameters are chosen to be the same as that of earlier studies [13,14,16]. This is equivalent to an experimental system of photons or atoms with an interaction quench which increases the interaction strength by a factor of 4, e.g., using a Feshbach resonance in the atomic case [21].

The resulting quantum dynamical equation of motion in the TW representation is

$$\frac{d\psi}{d\tau} = i\nabla_z^2 \psi - 2iC\psi(|\psi|^2 - 2\epsilon) + O(1/N), \tag{4}$$

where $\epsilon = 1/(2N\Delta z)$ is an ordering correction for a computational lattice spacing of Δz. The $O(1/N)$ term represents higher-order differential operators in the phase-space evolution equations, which are neglected here.

The quantum time-evolution dynamical equations in the positive-P case are [5]

$$\begin{aligned} \frac{d\psi}{d\tau} &= i\nabla_z^2 \psi - 2iC\psi^+ \psi^2 - i\sqrt{2iC}\psi\eta(\tau, z), \\ \frac{d\psi^+}{d\tau} &= -i\nabla_z^2 \psi + 2iC\psi^{+2}\psi - \sqrt{2iC}\psi^+ \eta^+(\tau, z), \end{aligned} \tag{5}$$

with independent complex Gaussian stochastic noises η, η^+, having nonvanishing correlations

$$\begin{aligned} \langle \eta(\tau, z)\eta(\tau', z') \rangle &= \langle \eta^+(\tau, z)\eta^+(\tau', z') \rangle \\ &= \delta(\tau - \tau')\delta(z - z')/\sqrt{N}. \end{aligned} \tag{6}$$

The partial differential equations were solved using an interaction picture fourth-order Runge-Kutta method, using two different public-domain software packages [43,44], with identical results. Most results given here use the approximate TW method, as it has much lower sampling error for long times in this system. These were replicated up to the first oscillation peak with the positive-P equations, as a check on the method.

A similar calculation has been performed in Refs. [16,34]. This demonstrated that all four local conservation laws are satisfied in the simulations. The time evolution of the density of the classical soliton system near the center ($z = 0$) oscillates with constant period. However, the true quantum condensate fragments into smaller Bose condensates. Thus, the soliton gradually breaks up, causing quantum fluctuations on macroscopic scales.

Here we investigate the quantum correlations caused by this instability, and their behavior in the large N limit. To do this we investigate soliton experiments with different number of particles N while keeping C constant, so the classical results are the same due to the scaling factor used

to define the dimensionless fields. We note that the characteristic $1/N$ scaling of the quantum noise terms leads to the expectation that quantum noise driven instabilities will occur more slowly at larger particle number.

Defining $n_i = n(z_i) \equiv |\psi(z_i)|^2$, the measurable quantum correlations are given by the second-order intensity correlation $G^{(2)}(z_1, z_2) = N^2\langle\hat{\psi}^\dagger(z_1)\hat{\psi}^\dagger(z_2)\hat{\psi}(z_2)\hat{\psi}(z_1)\rangle$ [45]. In terms of the Wigner ensemble averages, this is

$$G^{(2)}(z_1, z_2) = N^2\langle n_1 n_2 - \epsilon(1+\delta_{z_1 z_2})[n_1 + n_2 - \epsilon]\rangle_W. \quad (7)$$

The normalized correlation function is given by

$$g^{(2)}(z_1, z_2) = \frac{\langle\hat{\psi}^\dagger(z_1)\hat{\psi}^\dagger(z_2)\hat{\psi}(z_2)\hat{\psi}(z_1)\rangle}{\langle\hat{n}(z_1)\rangle\langle\hat{n}(z_2)\rangle}, \quad (8)$$

where we note that the product of annihilation and creation operators is expressed in terms of the Wigner representation, so that the scaled number density is

$$\langle\hat{n}(z)\rangle = \langle\hat{\psi}^\dagger(z)\hat{\psi}(z)\rangle = \langle n(z)\rangle_W - \epsilon. \quad (9)$$

The normalized correlation function is used to observe the bunching $[g^{(2)}(z,z) > 1]$ and antibunching $[g^{(2)}(z,z) < 1]$ amplitude of the soliton. According to the contour plot displayed in Fig. 1, for the $N = 10^3$ system, the 1D BEC soliton develops a strong bunching region with peaks of $g^{(2)}$ increasing from $\sim$1.1 at $\tau = 1.0$ [Fig. 1 (top)] to $\sim$2 at $\tau = 5.0$ [Fig. 1 (bottom)].

When using the normally ordered positive-P representation, the normally ordered averages require no ordering corrections. In this case, we define $n_i \equiv \psi^+(z_i)\psi(z_i)$, and one finds that $G^{(2)}(z_1, z_2) = N^2\langle n_1 n_2\rangle_P$, and $\langle\hat{n}(z)\rangle = \langle n(z)\rangle_P$. This method has no N-dependent truncation, which allows us to confirm that truncation errors are negligible in the Wigner predictions, at least up to the first peak. Figure 2 shows complete agreement of the two simulations with $N = 1000$, for $g^{(2)}(\Delta z) \equiv g^{(2)}(\Delta z/2, -\Delta z/2)$. This gives nonlocal anticorrelations and correlations at the first peak, occurring at $\tau = \pi/8$.

At larger N values of $N = 10^5$, the peak value of $g^{(2)}$ is significantly reduced to $\sim$1.1 at $\tau = 5.0$, which appears to give a weaker bunching within the soliton. Figures 3 and 4 show the time evolution of the nonlocal correlation, $g^{(2)}(\Delta z/2, -\Delta z/2)$ at different times, for $N = 10^3$ and $N = 10^5$, respectively. These graphs show that the strongest correlations occur near the peak intensities and are almost unchanged with particle number. What changes with N is the width in time of these correlations, as they remain strong for a much longer time with smaller particle number. The large anticorrelations at long times show that fragmentation occurs to a highly asymmetric output, with a much larger fragment occurring at $+z$ than at $-z$, or vice versa, leading to strongly negative correlations relative to the vacuum level.

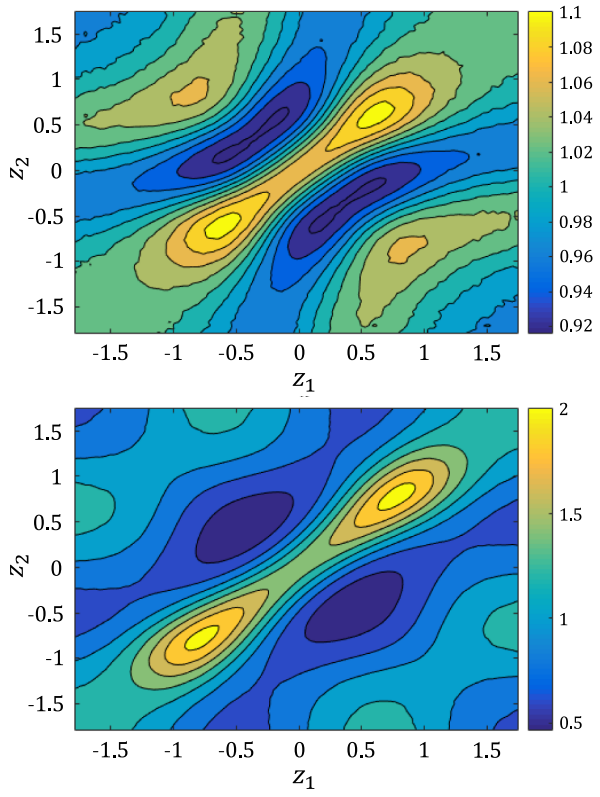

FIG. 1. Normalized second-order correlation $g^{(2)}(z_1, z_2)$ for $N = 10^3$ at $\tau = 1.0$ (top) and $\tau = 5.0$ (bottom). Here $C = -8$ and $L = 20$. Simulations have $M = 512$ modes, 9×10^4 trajectories, and 9×10^4 time steps. The contour plots show the region within $z = \pm 1.78$. The diagonal axis shows the local correlation $g^{(2)}(\bar{z}, \bar{z})$, with $\bar{z} = (z_1 + z_2)/2$. The antidiagonal axis shows the nonlocal correlation $g^{(2)}(z_1, z_2)$ where $z_1 = -z_2$. The maximum sampling error is 10^{-2} and the maximum time-step error is 10^{-6}.

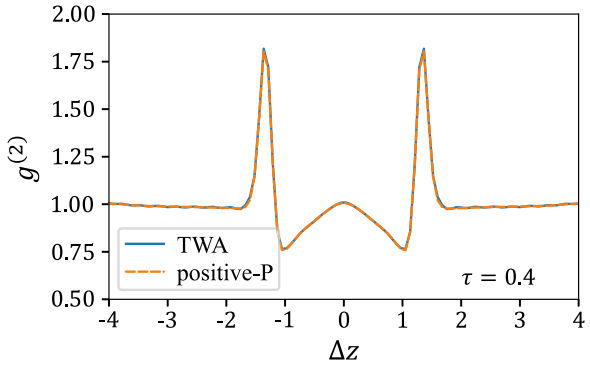

FIG. 2. Normalized second-order correlation $g^{(2)}(\Delta z) \equiv g^{(2)}(\Delta z/2, -\Delta z/2)$ for $N = 10^3$, $\tau = \pi/8$, $C = -8$. Simulations have $M = 512$ modes, 9×10^4 trajectories, and 9×10^4 time steps. Graphs compare calculations with the truncated Wigner (TW) method and exact positive-P representations, showing complete agreement within the width of the graphed lines.

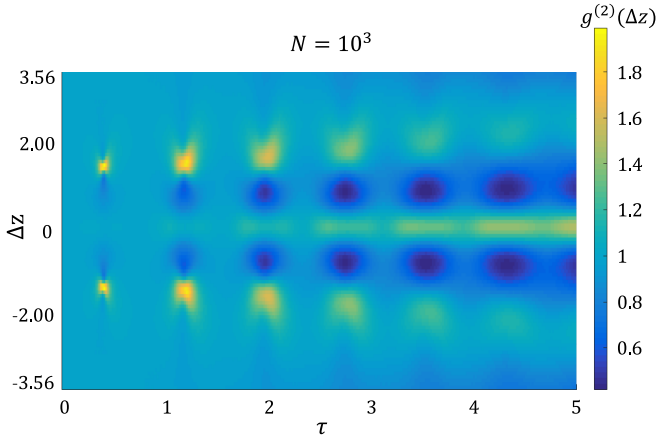

FIG. 3. Time evolution of the normalized second-order correlation $g^{(2)}(\Delta z)$, where $N = 10^3$, $C = -8$, and $L = 20$. Simulations with $M = 512$ modes, 9.6×10^4 trajectories, and 9×10^4 time steps. These contours correspond to the correlation along the antidiagonal axis in Fig. 1 which represent the nonlocal correlation. The maximum sampling error is around 0.2% of $g^{(2)}(\Delta z)$.

Next, we ask are these simply classical correlations, or do they have nonclassical, quantum features? Classical correlations obey the Cauchy-Schwarz inequality (CSI), which in terms of the second-order correlation functions, $G^{(2)}(z_1, z_2) = N^2\langle :\hat{n}(z_1)\hat{n}(z_2):\rangle = N^2\langle \hat{\psi}^\dagger(z_1)\hat{\psi}^\dagger(z_2)\hat{\psi}(z_2)\hat{\psi}(z_1)\rangle$, is given by

$$G^{(2)}(z_1, z_2) \leq \sqrt{G^{(2)}(z_1, z_1)G^{(2)}(z_2, z_2)}. \quad (10)$$

Quantum correlations have been demonstrated with matter waves using violations of the Cauchy-Schwarz inequality [27]. One can introduce a correlation coefficient $C_{\mathrm{CSI}} = G^{(2)}(z_1, z_2)/\sqrt{G^{(2)}(z_1, z_1)G^{(2)}(z_2, z_2)}$ to demonstrate that the system possesses nonlocal fluctuations that are stronger than any possible classical fluctuations, when $C_{\mathrm{CSI}} > 1$ [27,30,45,46]. For a system of identical bosons, the CSI is violated if the coefficient C_{CSI} is greater than unity. A violation also implies that entanglement exists [47]. In our simulations, we find small CSI violations (of order 10^{-3} at most) which may not be observable but are nonetheless suggestive of entanglement.

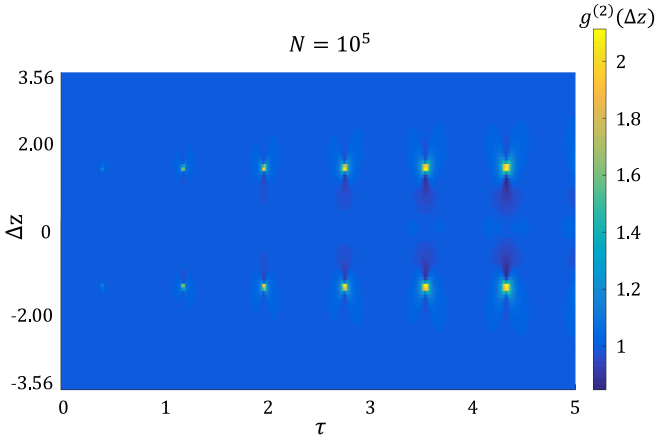

FIG. 4. Time evolution of the normalized second-order correlation $g^{(2)}(\Delta z)$, with $N = 10^5$. Other parameters as in Fig. 3.

In fact, we are able to illustrate the existence and origin of a very strong entanglement directly associated with the nonlocal correlations, given the BEC is a pure state. For a laboratory-prepared BEC, this is a good approximation. If we label the states for locations with $x < 0$ and $x \geq 0$ as $|\psi_-\rangle$ and $|\psi_+\rangle$, respectively, then entanglement exists between the subsystems at the two locations if it is not possible to write the state in the factorized form $|\psi\rangle = |\psi_-\rangle|\psi_+\rangle$. Owing to super-selection rules for massive bosons [48,49], the pure state for the system is in an eigenstate of total particle number $N_{\mathrm{tot}} = N_- + N_+$, $N_\pm$ being the particles with $x \gtrless 0$. Hence, in terms of number states $|n\rangle_\pm$ for the two locations, as $|\psi_N\rangle = \sum_{n=0,1,..}^{N} c_n|n\rangle_-|N-n\rangle_+$, where c_n are probability amplitudes. We see that there is always entanglement unless only one c_n is nonzero, in which case the number difference $\Delta N = \hat{N}_+ - \hat{N}_-$ is constant. Hence, a nonzero variance in the number-difference ΔN is an immediate proof of entanglement.

A typical number-difference variance result is shown in Fig. 5, using the exact complex P-representation method

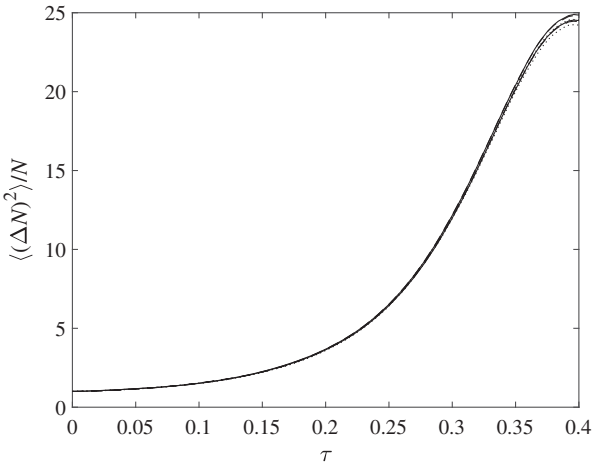

FIG. 5. Time evolution of the normalized number-difference variance, $\langle(\Delta N)^2\rangle/N$, with $N = 5 \times 10^3$, demonstrating creation of an entanglement due to states more widely separated in number difference with time. Here, $\langle\Delta N\rangle = 0$. The simulations have $M = 256$ modes, with 5×10^4 trajectories and 10^4 time steps. The two lines plotted are the $\pm\sigma$ bounds due to the finite sampling error. The solid lines use a pure initial number state and the exact complex-P representation. An initial Poissonian state gives virtually identical results, using either an exact positive-P integration (dashed lines), or the approximate Wigner method (dotted lines).

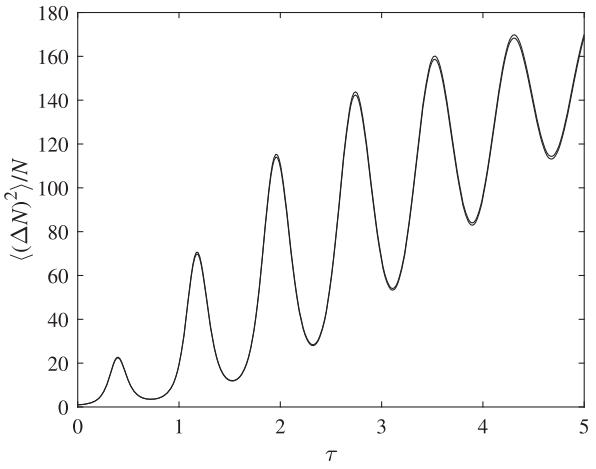

FIG. 6. Long time evolution of the normalized number-difference variance, $\langle(\Delta N)^2\rangle/N$, with $N = 10^3$, demonstrating oscillation and increasing weights in the entangled state $|\psi_N\rangle$ of states with a larger number difference ΔN. Simulations have $M = 256$ modes, 5×10^4 trajectories, and 3×10^4 time steps. The lines are from a Poissonian initial state integrated with the approximate Wigner method, as in the previous figure, with much longer time evolution.

with an initial pure number state. There is a small and nearly unobservable entanglement even initially, due to the nonlocal character of a pure Fock state. This rapidly grows by more than an order of magnitude at the first density maximum. Noting that $\langle \Delta N\rangle = 0$, the dramatically increasing variance in ΔN with time indicates an increased weighting in the entangled state $|\psi_N\rangle$ of states with a broader range of number difference ΔN. The associated entropy of entanglement given by $S = -\sum_n P(n)\log_2[P(n)]$ where $P(n) = |c_n|^2$ is also nonzero, but thus does not give information about the relative contributions of the states with different ΔN.

The calculation was carried out efficiently with a complex von Mises distribution for the initial P-function, as recently used to analyze boson sampling experiments [50,51]. These results also agree within sampling error with quantum simulations from a Poissonian initial condition, using either an exact positive-P or TW method.

Figure 6 shows how the normalized variance changes on much longer timescales. The approximate TW method is used for this, as the other methods have large sampling errors on long timescales. The two results plotted have N values that differ by a factor of 5, but nearly scale-invariant normalized correlations.

To summarize, our quantum dynamical calculations predict very strong nonlocal anticorrelations in 1D BEC soliton breathers as they fragment. The oscillatory decay of the nonlocal correlation depends on the particle number N, with the position and the amplitude of the correlation peak being relatively stable at large N, but with a reduced peak width. There is also an extremely strong nonlocal entanglement, as demonstrated by an exact positive-P simulation using both number state and Poissonian initial conditions. We interpret this as a generation of entangled, correlated pairs of daughter solitons, which starts to occur as soon as the first peak. At subsequent peaks we find that the correlation becomes even stronger, indicating that it should be readily observable.

P. D. D. and M. D. R. thank the Australian Research Council and the hospitality of the Institute for Atomic and Molecular Physics at Harvard University, supported by the NSF. P. D. D. acknowledges useful discussions with M. Olshanii and R. G. Hulet. This research has been supported by the Australian Research Council Discovery Project Grants schemes under Grant No. DP180102470.

[1] J. S. Russell, Report on waves, *Fourteenth meeting of the British Association for the Advancement of Science* (1845), pp. 311–390.
[2] D. J. Korteweg and G. de Vries, London Edinburgh Dublin Philos. Mag. J. Sci. **39**, 422 (1895).
[3] J. B. McGuire, J. Math. Phys. (N.Y.) **5**, 622 (1964).
[4] H. B. Thacker, Rev. Mod. Phys. **53**, 253 (1981).
[5] S. J. Carter, P. D. Drummond, M. D. Reid, and R. M. Shelby, Phys. Rev. Lett. **58**, 1841 (1987).
[6] P. D. Drummond and A. D. Hardman, Europhys. Lett. **21**, 279 (1993).
[7] H. A. Haus and Y. Lai, J. Opt. Soc. Am. B **7**, 386 (1990).
[8] M. Rosenbluh and R. M. Shelby, Phys. Rev. Lett. **66**, 153 (1991).
[9] P. D. Drummond, R. M. Shelby, S. R. Friberg, and Y. Yamamoto, Nature (London) **365**, 307 (1993).
[10] S. Spälter, N. Korolkova, F. König, A. Sizmann, and G. Leuchs, Phys. Rev. Lett. **81**, 786 (1998).
[11] J. F. Corney, J. Heersink, R. Dong, V. Josse, P. D. Drummond, G. Leuchs, and U. L. Andersen, Phys. Rev. A **78**, 023831 (2008).
[12] M. J. Werner, Phys. Rev. A **54**, R2567 (1996).
[13] A. I. Streltsov, O. E. Alon, and L. S. Cederbaum, Phys. Rev. Lett. **100**, 130401 (2008).
[14] J. G. Cosme, C. Weiss, and J. Brand, Phys. Rev. A **94**, 043603 (2016).
[15] V. A. Yurovsky, B. A. Malomed, R. G. Hulet, and M. Olshanii, Phys. Rev. Lett. **119**, 220401 (2017).
[16] B. Opanchuk and P. D. Drummond, Phys. Rev. A **96**, 053628 (2017).
[17] S. Coleman, Phys. Rev. D **15**, 2929 (1977).
[18] L. F. Mollenauer, R. H. Stolen, and J. P. Gordon, Phys. Rev. Lett. **45**, 1095 (1980).
[19] L. Khaykovich, F. Schreck, G. Ferrari, T. Bourdel, J. Cubizolles, L. D. Carr, Y. Castin, and C. Salomon, Science **296**, 1290 (2002).
[20] K. E. Strecker, G. B. Partridge, A. G. Truscott, and R. G. Hulet, Nature (London) **417**, 150 (2002).
[21] J. H. Nguyen, D. Luo, and R. G. Hulet, Science **356**, 422 (2017).
[22] E. P. Gross, J. Math. Phys. (N.Y.) **4**, 195 (1963).

[23] E. P. Gross, Il Nuovo Cimento **20**, 454 (1961).
[24] L. Pitaevskii, Soviet Physics JETP **13**, 451 (1961).
[25] T. P. Billam, S. L. Cornish, and S. A. Gardiner, Phys. Rev. A **83**, 041602(R) (2011).
[26] D. I. H. Holdaway, C. Weiss, and S. A. Gardiner, Phys. Rev. A **85**, 053618 (2012).
[27] K. V. Kheruntsyan, J.-C. Jaskula, P. Deuar, M. Bonneau, G. B. Partridge, J. Ruaudel, R. Lopes, D. Boiron, and C. I. Westbrook, Phys. Rev. Lett. **108**, 260401 (2012).
[28] M. Bonneau, W. J. Munro, K. Nemoto, and J. Schmiedmayer, Phys. Rev. A **98**, 033608 (2018).
[29] T. Wasak and J. Chwedeńczuk, Phys. Rev. Lett. **120**, 140406 (2018).
[30] M. D. Reid and D. F. Walls, Phys. Rev. A **34**, 1260 (1986).
[31] L. Rosales-Zárate, B. Opanchuk, P. D. Drummond, and M. D. Reid, Phys. Rev. A **90**, 022109 (2014).
[32] E. P. Wigner, Phys. Rev. **40**, 749 (1932).
[33] J. F. Corney, P. D. Drummond, J. Heersink, V. Josse, G. Leuchs, and U. L. Andersen, Phys. Rev. Lett. **97**, 023606 (2006).
[34] P. D. Drummond and B. Opanchuk, Phys. Rev. A **96**, 043616 (2017).
[35] P. D. Drummond and C. W. Gardiner, J. Phys. A **13**, 2353 (1980).
[36] C. Weiss and L. D. Carr, arXiv:1612.05545.
[37] S. E. Pollack, D. Dries, R. G. Hulet, K. M. F. Magalhães, E. A. L. Henn, E. R. F. Ramos, M. A. Caracanhas, and V. S. Bagnato, Phys. Rev. A **81**, 053627 (2010).
[38] E. H. Lieb and W. Liniger, Phys. Rev. **130**, 1605 (1963).
[39] R. J. Glauber, Phys. Rev. **131**, 2766 (1963).
[40] C.-S. Chuu, F. Schreck, T. P. Meyrath, J. L. Hanssen, G. N. Price, and M. G. Raizen, Phys. Rev. Lett. **95**, 260403 (2005).
[41] M. J. Steel, M. K. Olsen, L. I. Plimak, P. D. Drummond, S. M. Tan, M. J. Collett, D. F. Walls, and R. Graham, Phys. Rev. A **58**, 4824 (1998).
[42] B. Opanchuk and P. D. Drummond, J. Math. Phys. (N.Y.) **54**, 042107 (2013).
[43] S. Kiesewetter, R. Polkinghorne, B. Opanchuk, and P. D. Drummond, SoftwareX **5**, 12 (2016).
[44] B. Opanchuk, http://reikna.publicfields.net (2014).
[45] R. J. Glauber, Phys. Rev. **130**, 2529 (1963).
[46] R. Loudon, Rep. Prog. Phys. **43**, 913 (1980).
[47] T. Wasak, P. Szańkowski, P. Ziń, M. Trippenbach, and J. Chwedeńczuk, Phys. Rev. A **90**, 033616 (2014).
[48] G. C. Wick, A. S. Wightman, and E. P. Wigner, Phys. Rev. **88**, 101 (1952).
[49] B. Dalton, J. Goold, B. Garraway, and M. Reid, Phys. Scr. **92**, 023004 (2017).
[50] B. Opanchuk, L. Rosales-Zárate, M. D. Reid, and P. D. Drummond, Phys. Rev. A **97**, 042304 (2018).
[51] B. Opanchuk, L. Rosales-Zárate, M. D. Reid, and P. D. Drummond, Opt. Lett. **44**, 343 (2019).